Smart Structures and Systems, *Vol. 14, No. 5 (2014) 765-784*
DOI: http://dx.doi.org/10.12989/sss.2014.14.5.765

Performance analyses of antagonistic shape memory alloy actuators based on recovered strain

Zhenyun Shi*, Tianmiao Wang and Liu Da

Robotic Laboratory, BeiHang University, HaiDian District, 37 XueYuan Road, Beijing 100191, China

(Received April 18, 2013, Revised October 10, 2013, Accepted October 16, 2013)

Abstract. In comparison with conventional shape memory actuated structures, antagonistic shape memory alloy (SMA) actuators permits a fully reversible two-way response and higher response frequency. However, excessive internal stress could adversely reduce the stroke of the actuators under repeated use. The two-way shape memory effect might further decrease the range of the recovered strain under actuation of an antagonistic SMA actuator unless additional components (e.g., spring and stopper) are added to regain the overall actuation capability. In this paper, the performance of all four possible types of SMA actuation schemes is investigated in detail with emphasis on five key properties: recovered strain, cyclic degradation, response frequency, self-sensing control accuracy, and controllable maximum output. The testing parameters are chosen based on the maximization of recovered strain. Three types of these actuators are antagonistic SMA actuators, which drive with two active SMA wires in two directions. The antagonistic SMA actuator with an additional pair of springs exhibits wider displacement range, more stable performance under reuse, and faster response, although accurate control cannot be maintained under force interference. With two additional stoppers to prevent the over stretch of the spring, the results showed that the proposed structure could achieve significant improvement on all five properties. It can be concluded that, the last type actuator scheme with additional spring and stopper provide much better applicability than the other three in most conditions. The results of the performance analysis of all four SMA actuators could provide a solid basis for the practical design of SMA actuators.

Keywords: shape memory alloy; performance; antagonistic structure; actuator design; recovered strain

1. Introduction

NiTi shape memory alloy (SMA) exhibits a crystal phase transition up to or below a critical temperature, which causes it to change between the austenite phase and martensite phase (Otsuka and Wayman 1998). Below the martensite starting temperature (Ms), the SMA structure has low stiffness and inelastic straining (Otsuka and Wayman 1998); above the austenite starting temperature (As), the shape memory effect (SME) appears by eliminating the de-twining strain, and the austenite structure appears with elastic modulus close to 100 GPa (Dynalloy, Inc). Moreover, the maximum recoverable strain can be higher than 5%.

In recent years, with the growing demand for miniaturization of actuation device in optical engineering, medical operations, and precision machining, SMA actuators have been developed to

*Corresponding author, Ph. D., E-mail: shichong1983623@hotmail.com

http://www.techno-press.org/?journal=sss&subpage=8 ISSN: 1738-1584 (Print), 1738-1991 (Online)

possess the following characteristics: high energy density, specific power, and ease of fabrication (Lan 2010). Reciprocating motion has been achieved in different structures, such as passive elastic force by spring (Lan and Yang 2009, Kyung *et al*. 2008, Sreekumar *et al*. 2008, Song 2007) or antagonistic pair wires (Teh and Featherstone 2008, Kohl *et al*. 2000, Wang *et al*. 2008, Bundhoo *et al*. 2008). However, all applications of SMAs are inhibited by the hysteresis, slow response, and cyclic degradation. Hysteresis can be compensated by exterior and interior feedback control and a feed-forward strategy (Ma *et al*. 2004, Wang *et al*. 2012). The response time of the SMA can be shortened by a cooling system (Romanno and Tannuri 2009), repeat heating with resistance feedback (Schiedeck and Mojrzisch 2011), or antagonistic actuation (Teh and Featherstone 2008, Bundhoo *et al*. 2008, Lan and *et al*. 2009). Cyclic degradation can be improved by properly pre-straining (Solfa *et al*. 2008).

In contrast to conventional SMA devices that require bias force components, antagonistic SMA actuators with more than two SMA units show fully reversible responses in both directions (Duerig *et al*. 1990) as well as higher frequency response, which hold promise for wide applications. They can be largely categorized into four types of SMA actuator design, as shown in Fig. 1. Since one-way SMA wires can only provide pulling force, a spring or an antagonistic unit is necessary to supply the restoring force. As shown in Fig. 1(a), in conventional SMA devices, it includes one SMA wire with spring (is called SWS), the spring could offer passive force to the SMA wire over the entire duration; however, the force is attenuated according to the increase in strain on the wire. Under this condition, the induced residual displacement cannot be avoided, thus the response speed becomes rather slow under the insufficient passive force. As shown in Fig. 1(b), placing another SMA wire instead the spring (is called AW) could supply higher restoring force from actuating the wire. Hence, with two antagonistic wires, AW actuator has two-way motion with less residual displacement. Moreover, the response speed is increased and well controlled through the control strategy of both wires (Teh and Featherstone 2008, Wang *et al*. 2012). However, in this antagonistic wire system, even though the wires can be prestrained higher than 5% at the onset, after one heating cycle on both wires is applied (although not at the same time), and the wires will still slacken after cooling. This slackening of SMA wires is called the two-way shape memory effect, which has been explained by Kohl (2004), who also found that once this property started to appear, the wires are actively lengthened when cooled, even without a tension force. Part of the SMA recovered strain has to be consumed to tighten the wires prior to actuation. Higher pre-straining might keep the wires taut for a longer term, but a greater pulling stress is required to stretch the passive wire, which creates the stress-induced martensite in the driving wire (Lan *et al*. 2009); thus, phase transformation cannot be completed in this case. The actuation stroke becomes less under both conditions.

To prevent the slacken of SMA wires, a series spring in each wire is added for improved performance, two antagonistic wires-springs comprise the AWS actuator as shown in Fig. 1(c). With proper prestraining the springs can prevent slackening and over-stressing simultaneously, although part of the recovered strain on both wires is used to stretch the springs (Lan *et al*. 2009). To augment the working distance, a mechanical stopper can be attached to the spring, which is used to limit the over-extension of the springs, by combining a pair of antagonistic wires-springs-stoppers. The AWSS actuator is shown in Fig. 1(d). Based on this idea, Vishalini (Bundhoo *et al*. 2008) designed biomimetic artificial fingers, which used the stopper and spring as the tendon, and the SMA actuator as muscles.

Based on the discussion above, it can be concluded that: (1) the two-way actuation capability makes the antagonistic actuators with wider displacement range and higher frequency, which is

suited to actuator design (b), (c), and (d); (2) the additional components reduce the effect of the two-way shape memory effect which shows potential to further optimize the displacement range. In this case, the actuator design (c), (d) should be considered; (3) the antagonistic design and the additional components altered the internal stress state between the wires which make the cyclic degradation become uncertain, the effect to the actuator design (b), (c), and (d) is significant; and (4) the diversity of the extra stopper also apply on the control accuracy under external interference, while the additional components show magnitude difference from the SMA wires on the stiffness, all four actuators therefore display extreme differentiation controllable maximum output. Further research will be carrying out based on these essential differences.

Except for type (a), the remaining all three actuator schemes achieve two-way motion. In a practical actuator design, the actuator type should be chosen according to its suitability for the performance and the system requirement. Here they are five major properties highly related to the performance: recovered strain; cyclic degradation; responding frequency; self-sensing control accuracy; and controllable maximum output. Active displacement influences the compactness of the whole structure. The SMA actuator might be required to perform many cycles (Hornbogen 2004), and the strains recovered are always degraded in tens of cycles, a standard training procedure to achieve stable performance is the foundation of the application. Response frequency is an important evaluation criterion of the actuator property. The employed self-sensing could maximally reduce the amount of additional sensors. The description of the strain-electrical resistance (S-R) hysteresis curve is the basis of accurate self-sensing control, and controllable maximum output affects the applicability of the actuator.

In this paper, all four types of SMA actuators design are examined in detail, the three units with two-way motion in particular. A special testing platform was set up, which enables in carrying out tests of all types of actuators. The five properties that influence the performance were studied in detail. According to the merits and deficiencies, the design scheme of the SMA actuator can be easily determined.

Section 2 describes the experimental setup of the testing platform. The driving methodologies of four actuators are deduced in Section 3. In Section 4, comparisons of the five major properties on four actuators are carried out. In Section 5, based on the results, the strategy for the SMA actuator design scheme is established and presented in the conclusions which as drawn from this study.

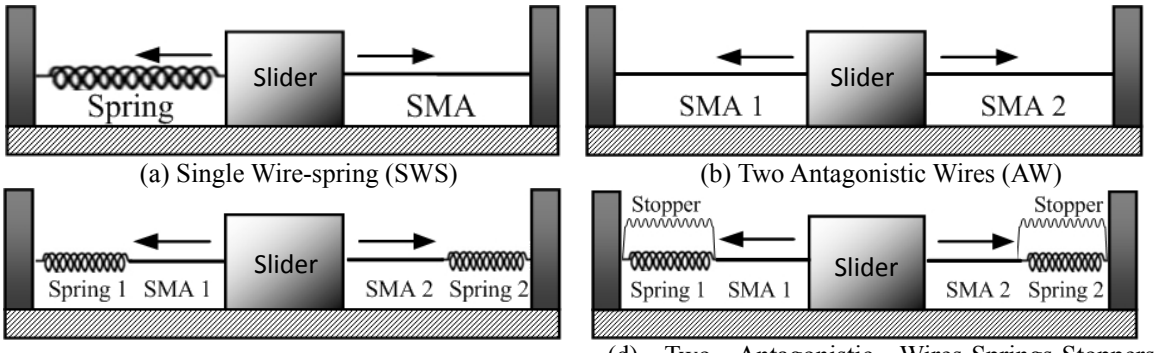

(a) Single Wire-spring (SWS)

(b) Two Antagonistic Wires (AW)

(c) Two Antagonistic Wires-springs (AWS)

(d) Two Antagonistic Wires-Springs-Stoppers (AWSS)

Fig. 1 Four Types of SMA actuators with additional components

2. Experimental setup

To study the properties of different SMA actuators, a testing platform was setup as shown in Fig. 2. Four sliders (one slider with a load cell) and another fixed load cell were installed on the linear bearing, and a pair of V-shaped (the two ends of the SMA wires are connected with one unit), 450mm long TiNi-based Flexinol®-LT SMA wires with 0.381mm in diameter were connected by clamps between the slider and load cell. The V-shaped wire is approximated as two 220 mm straight wires after ignoring the small angle caused by the screw. A linear bearing keeps both sliders moving horizontally. Two stoppers were installed between the two sliders at both ends, which have a minute adjustment system. A load cell is attached to one wire to measure the contraction force δ. A linear variable differential transformer (LVDT) position sensor with 10μm resolution, the tip of which is placed against the middle slider, is used to sense the displacement of the actuator. Notice that the LVDT sensor was used to construct the S-R modulus and validate the control result, but not to feed the signal back to the controller.

Electric power is used to drive the SMA wires, and a circuit shown in Fig. 3 is connected by two ends of the SMA wires. A multifunction data acquisition card (±10 V full-scale range, 18-bit resolution; PCI-6284, NI) is employed to send the PWM signal via the digital output and measure the actual voltage across the external resistor, V_R and the voltage across the SMA, V_{SMA} via the analog input. A Darlington driver is used as a switching element to control the heating or cooling state of the SMA actuator. An external resistor R0 is connected serially to the SMA actuator, which is used to measure the standard resistance.

Electric power is used to drive the SMA wires, and a circuit shown in Fig. 3 is connected by two ends of the SMA wires. A multifunction data acquisition card (±10 V full-scale range, 18-bit resolution; PCI-6284, NI) is employed to send the PWM signal via the digital output and measure the actual voltage across the external resistor, V_R and the voltage across the SMA, V_{SMA} via the analog input. A Darlington driver is used as a switching element to control the heating or cooling state of the SMA actuator. An external resistor R0 is connected serially to the SMA actuator, which is used to measure the standard resistance.

All resistance values discussed below are the proportional resistance values between the SMA and the external resistor.

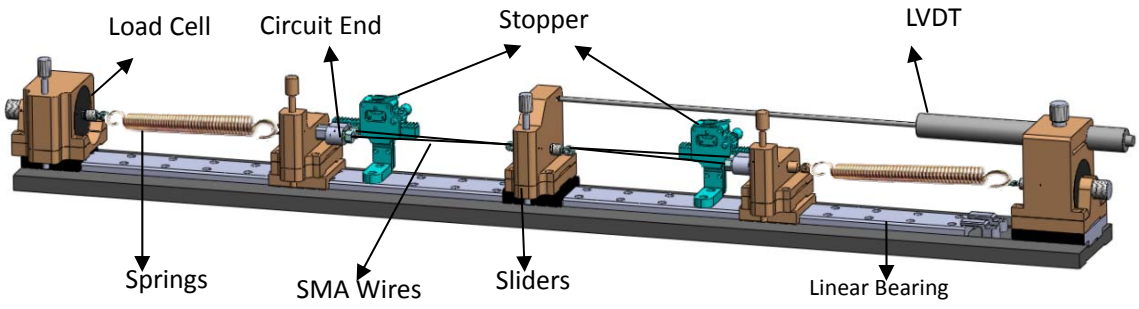

Fig. 2 Diagram of experimental setup: the platform

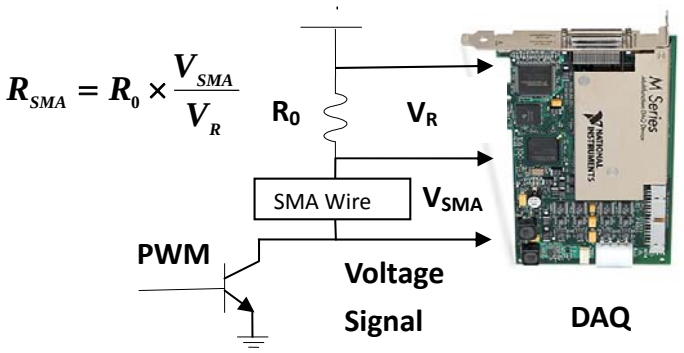

Fig. 3 Schematic of the electric circuit

3. Driving methodology analysis

3.1 SWS actuator

In the SWS actuator, the stiffness of the spring is kept constant, and the overall length of the spring and the wire does not change. The SWS actuator driving procedure is described below in Fig. 4:

As described in Figure 4, the spring is stretched driven by the SMA wire, and the recovered strain degrades after several cycles, related to the contribution of dislocation to the deformation incurred during each loading cycle (Gall and Maier 2002).

Previous studies (Lan *et al*. 2009, Lan and Fan 2010) have shown that with proper pre-straining, the stiffness of the spring does not have a significant effect on the S-R curve, but it does influence the recovered strain because over-stress might inhibit the austenitic phase transformation. Extending the recovered strain requires the application of greater stress on the SMA wire in the martensitic phase in order to pull it longer, and it requires smaller stress in the austenitic phase to sustain its transformation. The constant stiffness of the spring causes the pulling stress to be higher in the austenitic than in the martensitic phase. In this case, the spring with lower stiffness shows the advantage of increasing the stress in a narrow range under the same displacement. On the other hand, while the stress between the spring and wire increases with the pre-stress, which might increase the degradation speed of the shape memory property.

3.2 AW actuator

In the AW actuator, the driving wire is always transformed from the martensite to austenite phase, which cooperates with the passive wire under opposite transformation. After the pre-set, because the overall lengths of the wires in the actuator do not change, the austenite phase transformation is difficult to complete under such large inner stress. Furthermore, as we described in the introduction, no matter how large an amount of pre-strain has been applied, both wires will slacken after cooling down. Following this condition, the AW actuator driving procedure is described below:

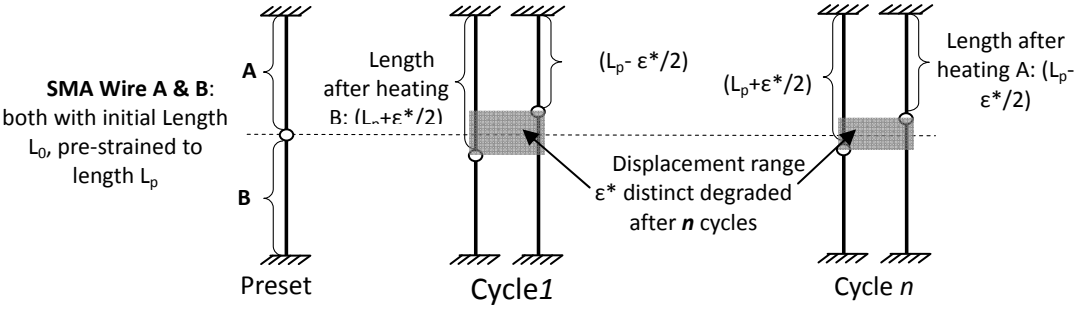

Fig. 5 The **AW** actuator test procedure and the active displacement range degrading process

As Fig. 5 shows, one SMA wire drives as the active wire while the passive wire is cooling down. The movements of the two wires are symmetrical, including the S-R relationship. The recovered strain degrades after several cycles for the same reason.

The principle of extending the recovered strain of the AW actuator does not differ from the SWS actuator, although the passive unit was changed from the spring to the cooled SMA wire, and the displacement range is clearly increased by the pre-tension strain.

3.3 AWS actuator

In the AWS actuator, the driving procedure of the driving and passive wire is identical to in the AW actuator, but the overall lengths of the wires in the actuator change with the driving procedure. The springs serve to lessen the stress between the two wires so that austenite phase transformation can be completed, although the stroke of each wire also stretches both springs in addition. The AWS actuator driving procedure is described below:

As described in Fig. 6, the SMA wires took turns as the driving wire, and the springs are both extended under stress. In each cycle, the displacement range degraded less by the reduced inner stress. As discussed, the springs serve to lessen the inner stress which assists to complete the austenite phase transformation, although the springs reduced the recovered strain. Also it was difficult to determine whether there was any tendency towards spring stiffness affecting the displacement range. To understand the effect of spring stiffness on the recovered strain, a group of testing focus on different spring stiffness has been carried out.

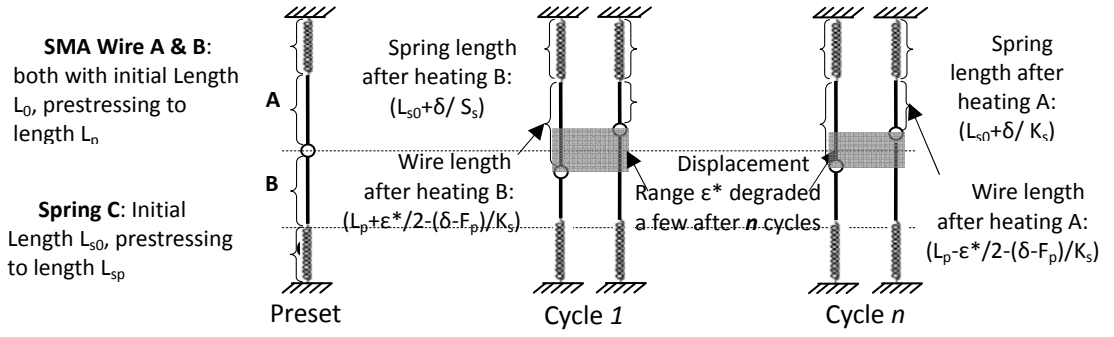

Fig. 6 The AWS actuator test procedure and the active displacement range degrading process

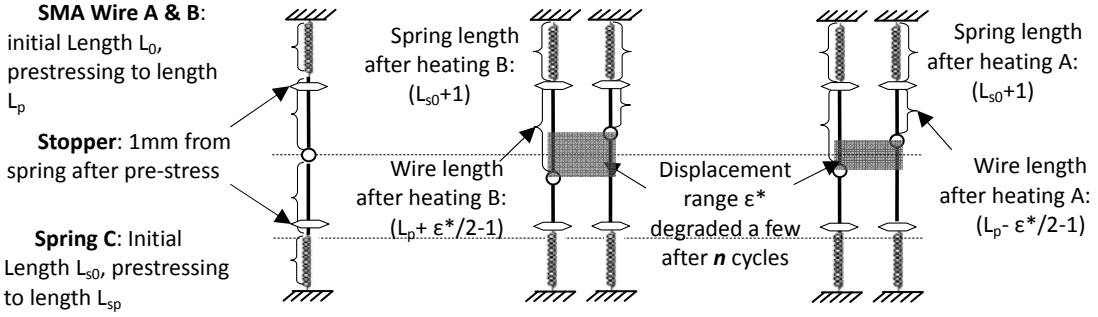

Fig. 7 The AWSS actuator test procedure and the active displacement range degrading process

3.4 AWSS actuator

The driving procedure of the AWSS actuator, can be separated into two stages: 1) Before the SMA wires bring the springs into contact with the stoppers, the working principle is same as the AWS actuator: the spring keeps applying prestress on both wires and extends when the wire strokes. 2) After the spring is resisted by the stopper, the working principle becomes the same as that of the AW actuator, which makes the inner stress between the wires much greater. In this structure, slackening of the SMA wires has been eliminated, and the stroke of each wire will not stretch the springs in addition. The AWSS actuator driving procedure is described below:

As described in Fig. 7, the SMA wires took turns as the driving wire, and the extension of springs was resisted by the stoppers. The recovered strain degraded similar to the AW actuator. The original gap between the stopper and the sliders is set to be less than 1mm at both sides. As discussed, the springs serve to eliminate the slackness of the wires at the first stage, and the stopper resists the extension of the springs at the second stage. The stopper's existence also makes the effect of the spring stiffness is no longer a concern.

4. Macroscopic properties analysis of actuators (results and discussion)

In real applications, five major macroscopic properties determine the applicability of SMA actuators: recovered strain; cyclic degradation; responding frequency; self-sensing control accuracy; control accuracy under external interference (controllable maximum output).

In the five key performance measures, it was believed that the recovered strain is increased following the order from type (a) to type (d) (Lan *et al*. 2009), although none of quantitative measurement have been done, which is important for actuator selection and design. The same status is with the response frequency analysis, antagonistic actuators are considered to respond faster, but specific promotion and limitation is still not understood. There are some researches about the cyclic degradation of the antagonistic actuators have been applied (Sofla *et al*. 2008), which focuses more on the function of pre-strain. The influence of the accumulation of irreversible strain by the on-time inner stress have not been further investigated, it is hard to know the cyclic degradation performance of each actuators without further research. Based on the self-sensing

control strategy, controllable maximum output becomes a key parameter for a smart actuator, which is undefined for four actuators with their individual components. In summary, no sufficient quantitative research have been done on these five properties to these four SMA actuators, which deem necessary to have a comprehensive evaluation for providing a rigorous base for applications. Comparisons of the five properties with four types of actuators are presented below.

4.1 Recovered strain

As discussed above, a wider displacement range of SMA could improve the compactness of the whole framework. In our experiments, all actuators were tested with Flexinol®-LT SMA wires with 220 mm original length. Within the antagonistic actuator, two SMA wires take turns working as the driver, and the recovered strain is the relative value of the displacement value between the boundaries positions in two directions divided by 220 mm. The test sets varied based on the features of different actuators, which are described in section 4.1.1.

4.1.1 Parameter setting

The difference between the parameter setups of the actuator are caused by the difference in stiffness between the wires and springs. The degrees of stiffness of the applied springs are listed in Table 1.

For the SWS actuator, the experiments were carried out under different pre-stresses and by comparing low spring stiffness. Springs with five degrees of stiffness were used to achieve good recovered strain, and a 22N, 28 N pre-stress was applied to the wires.

For the AW actuator, because pre-stressing cannot be applied to the wires at the beginning pre-strain of 5%, 5.6%, 6.2%, 7.2%, and 8% pre-strain were applied to the original length of the wire in order to compare their effects.

For the AWS actuator, the pre-strain of two wires is related to the pre-stress applied to the spring after the wires were original stretched to straighten them. To avoid the spring being stretched too easily while one wire contracts, the spring needs to have a sufficient degree of stiffness. The testing was done using the parameters of the study results on the actuator of the pair of antagonistic wires. Before the springs were stretched, the pre-strain was used as the basic parameter, and 7.2% pre-strain was applied to eight sets of springs in the test. After the springs were stretched, 8 N, 13 N, 20 N of pre-strain were applied。

As discussed in section 3.4, the working strategy of the AWSS actuator can be separated into two stages. The stiffness of the spring affects the recovered strain slightly. Testing parameters similar to the AWS actuator were used for the test, less groups of springs needed to be tested.

Table 1 Stiffness of applied spring

Spring	S1	S2	S3	S4	S5	S6	S7	S8
Stiffness (N/cm)	5.88	20.8	31.7	40.5	55.6	72.7	90.9	137.1

4.1.2 Recovered strain analysis

At the beginning, primary study of the effect of spring stiffness and pre-stress was carried out on the SWS actuator. As shown in Table 2, recovered strain was achieved with the spring and the corresponding pre-stress. Note all the data filled into the tables is taken from the average value of three groups tests.

As Table 2 shows, when the pre-stress is high enough, springs with low stiffness can achieve a wider displacement range. The data also shows that highly stiff springs under high pre-stress may lead to overstressing, which stops the transformation. Based on these results, it is concluded that stress on35N (inner-stress with S 3 under 22N pre-stress) significantly influenced the memory property of SMA wires by preventing phase transformation. Thus, over-stressing will be carefully avoided in the future.

Compared with the SWS actuator, the AW actuator is driven by two SMA wires, which have nonlinear stiffness caused by phase transformation. The two-way shape memory effect makes the inner stress between the two wires even more complicated. Because of the slackening of the wires, instead of pre-stress, pre-strain was applied to the actuator. As shown in Table3, 5%, 5.6%, 6.2%, 7% and 8% pre-straining was applied to the wires in order to compare their effects.

From the understanding of SMA wire, insufficient pre-strain causes the memory property of the SMA to malfunction; in addition, over-strain could lead to over-stress, which stops the phase transformation. As shown in Table 3, a pre-strain of 7.2% shows the largest recovered strain, although some over-stress is indicated, which makes the cyclic degradation analysis of both 6.2% and7.2% pre-straining necessary.

As discussed in section 3.3, the AWS actuator works according to principles that are different from other actuators. The springs are required to have sufficient stiffness to avoid over-extension when one SMA wire is driving. However, too much stiffness might lead to over-stress between the wires. As shown in Table4, the recovered strain of the AWS actuator under different degrees of pre-strain and springs was tested.

The results show that in most cases, the recovered strain increases with increased pre-stress (7.2 % pre-strain was treated as zero pre-stress). However, it is also found that when the inner force was large enough to stop phase transformation, the memory property of SMA degraded quickly in each cycle, which is discussed in section 4.2. As Table 4 shows, the recovered strain values, which are in bold and starred are the best achieved values just before wires become over-stressed.

Table 2 Recovered strain under different springs and pre-stress within SWS actuator

Pre-stress and Spring	S1	S2	S3	S4	S5
22N	4.62%	*4.64%	4.6%	4.55%	4.4%
28N	*4.85%	4.62%	4.57%	4.5%	4.3%

Table 3 Recovered strains under different pre-strain within AW actuator

Pre-strain	5%	5.6%	6.2%	7.2%	8%
Recovered strain	4.11%	4.45%	*4.8%	*5.14%	5.18%

Table 4 Recovered strain under different pre-stress and springs within the AWS actuator

Spring	7.2% Pre-strain	8N Pre-stress	13N Pre-stress	20N Pre-stress
S1	3.67%	4.05%	4.30%	4.41%
S2	4.12%	4.36%	4.44%	4.64%
S3	4.46%	4.66%	4.74%	4.84%
S4	4.57%	4.71%	4.79%	*4.92%
S5	4.60%	4.76%	*4.88%	5.03%
S6	4.66%	4.87%	*4.97%	5.08%
S7	4.70%	*4.91%	5.02%	5.11%
S8	4.79%	*4.97%	5.10%	5.15%

As discussed in section 3.4, the driving process of the AWSS actuator was separated into two stages. Inner stress always jumps when changing from stage one to stage two, which is caused by the significantly higher stiffness of martensite SMA wires than that of the springs. Moreover, the pre-stress applied to the actuator by the spring does not need to be active because it only keeps the SMA wires in tension during the entire process. Actually, if the pre-stress is too high, it might lead to over-stress in the second stage between the wires, decreasing the recovered strain. The active degrees of strain of AWSS actuator according to different springs are listed in Table 5.

As Table 5 shows, the recovered strains of the AWSS actuator are kept at a very stable level even with different degrees of stiffness in the spring. Sufficient pre-stress (8N) kept the recovered strain at a good value, avoiding both over-stress and slackening of the wire.

Results of the testing of the four actuators are as follows: The SWS actuator had the narrowest recovered strain bound and thus needed to use a spring with low stiffness and proper pre-stress to achieve higher value. The AW actuator achieved good recovered strain with a convenient pre-strain. With highly stiff springs and matching pre-stress, the AWS actuator achieved its optimized recovered strain. The AWSS actuator was quite flexible in the selection of springs if the pre-stress was set correctly. Three antagonistic actuators showed quite impressing properties in recovered strain. The text for cyclic degradation testing further proved their recovered strain in additional cycles.

Table 5 Recovered strain under different pre-strain and springs within the AWSS actuator

Spring	7.2% Pre-strain	8N Pre-stress	13N Pre-stress	20N Pre-stress
S1	4.69%	*4.99%	5.02%	5.03%
S2	4.69%	*4.99%	5.02%	5.03%
S3	4.69%	*4.99%	5.02%	5.03%
S4	4.69%	*4.99%	5.02%	5.03%
S5	4.69%	*4.99%	5.02%	5.03%
S6	4.69%	*4.99%	5.02%	5.08%

4.2 Cyclic degradation

In real applications, because actuators need to perform many cycles (Hornbogen 2004), SMA devices be capable of repeatedly undergoing the martensite de-twinning process (to accommodate pre-strain), followed by a martensite to austenite transformation (Duerig 1990).However, the repeated use of SMA devices could result in a dramatically diminished stroke of the load-supporting SMA wires (Furuya 1988, Furuya 1989).The recovered strain reduction is believed to be related to the contribution of dislocation to the deformation incurred during each loading cycle (Scherngell 1998). Moreover, applied stress, which effects the stabilization of the martensite variants, has been proved to contribute to cycle degradation (Gall and Maier 2002, Furuya 1988). The residual elongation of a SMA linear actuator can contribute to further reduction in displacement reduction, which causes the pre-strain to become another crucial influence.

This reduced-shape memory strain results in a diminished recovered strain in the actuators, but the reduction of each actuator shows various characteristics, which is caused by distinct inner stress relationships. Regarding the boundary of the recovered strain in two directions, the single SMA-spring actuator and the antagonistic SMA actuator have different features, as shown in Fig. 8, which illustrates that the rate of reduction of the strain range decreases during cycling loading.

To investigate the cyclic degradation for each actuator, the experiments were repeated over1000 complete cycles to study the inactive strain of pre-strained or pre-stressed shape memory actuators. The initial parameters (pre-strain, pre-stress and spring stiffness) were chosen according to the conclusion given in section 3, which showed the best initial recovered strain. In this research, cycle 1000 was chosen as the cutting-off cycle for all data points because the recovered strain value always becomes similar to the antagonistic SMA-wires actuator under different degrees of spring stiffness and pre-stress. To make the comparison more distinct, the absolute value of the recovered strain is used in the analysis. The reduction in the recovered strain of each actuator under different pre-strain or pre-stress is achieved as shown in Fig. 9.

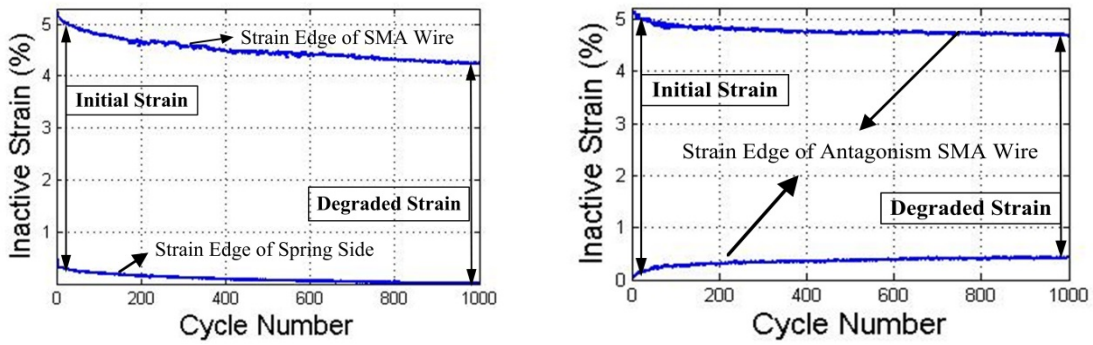

(a) Pre-stressed SWS actuator (b) Pre-strained antagonistic shape memory actuator

Fig. 8 The recovered strains (Inactive strain are shown) are degraded over 1000 cycles

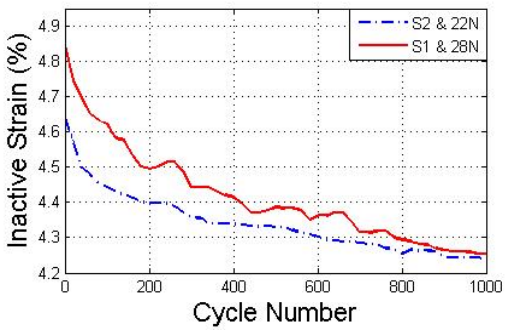

(a) Pre-stressed SWS actuator

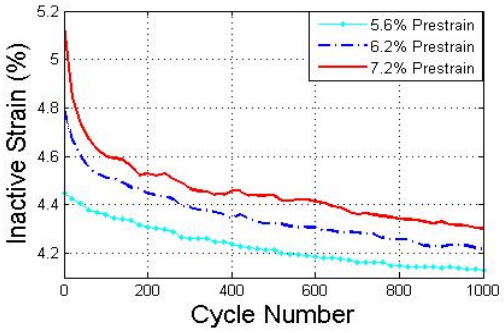

(b) Pre-strained AW actuator

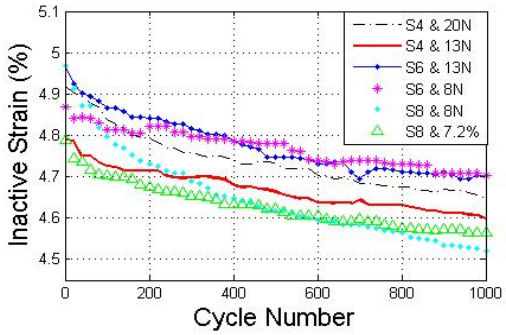

(c) Pre-stressed AWS actuator

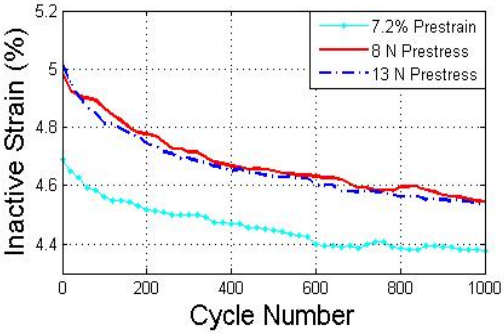

(d) Pre-stressed AWSS actuator

Fig. 9 The degradation of absolute value of recovered strain(Inactive strain are shown) tested over 1000 cycles

Fig. 9 illustrates the cyclic degradation of the recovered strain in four actuators. In both SWS and AW actuators, larger pre-stress or pre-strain improves both the initial working range and the final working range at the same time, until over-stress prevents the phase transformation and leads to quick degradation. However, in the AWS actuator, spring stiffness becomes the key factor of the working range: the results showed that insufficient or excessive spring stiffness could lead to narrow recovered strain. With the appropriate spring (S6), a wider working range and less degradation were achieved at the same time. According to the conclusion of section 3.4, because spring stiffness does not affect the AWSS actuator, suitable pre-stress (8N) is enough to increase the recovered strain and control the inner stress. To compare the degradation conditions of four actuators horizontally, the degradation curves under the optimized parameters of four actuators are compared below:

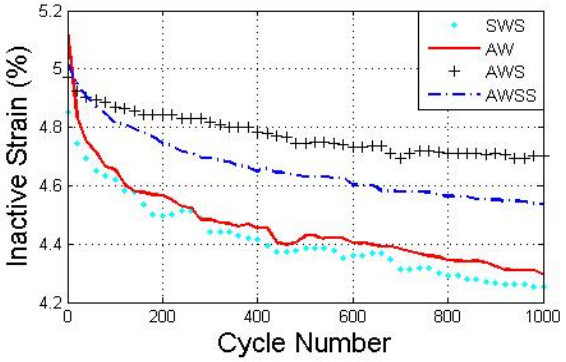

Fig. 10 The degradation of absolute value of recovered strain for four actuators under optimized parameterare tested over 1000 cycles

Fig. 10 shows that even with optimized parameters, SWS and AW actuator still cannot avoid substantial degradation to achieve better inactive strain. In comparison, the AWS and AWSS actuators degrade much less with a good initial recovered strain. In particular, the magnitude of the degradation of the AWS actuator can be almost ignored after 30 cycles.

4.3 Response frequency

In the conventional actuator system, the response frequency is hampered by the cooling speed of the SMA wires, which is driven by a spring with constant stiffness. In the antagonistic SMA wires actuator, the SMA wires provide two-way active driving, which increases the responding speed, even though the limitation of the cooling speed of the passive wire is still unsolved. To determine the improvement of the antagonistic SMA-wires actuator in responding frequency and limitations, a voltage from 7.5 V to 10 V was applied to heat the wires until the limitation of recovered strain was reached.

Fig. 11 summarizes the effect of the increased voltage (or by adjusting the duty ratio) on the responding speed of a whole cycle. The responding speed with the antagonistic actuator is symmetrical in two directions and strain-time curve of one direction is sufficient. However, the responding speed of the SWS actuator varies in two directions, and the strain-time curves of two directions were attached.

In the SWS actuator, the contraction speed of the SMA wire was increased with nearly unlimited voltage, but it took more than 15s to cool down in order to achieve 90% extension, which limited its frequency to less than 0.065 Hz. In the antagonistic actuator, the SMA wire exerted larger force to pull the passive wire, which increased the responding frequency to higher than 0.13 Hz, achieving more than 90% active strain. The responding speed increased slightly after the voltage increase beyond 9V. The cooling speed of the SMA wire must still be considered the limiting factor in responding speed, which indicates that an extra cooling component is the best solution. Of all three antagonistic actuators, only the AWS actuator showed the following feature: when the applied voltage was more than 8V, the responding speed was reduced, the major cause of which seemed to be the extension of the springs.

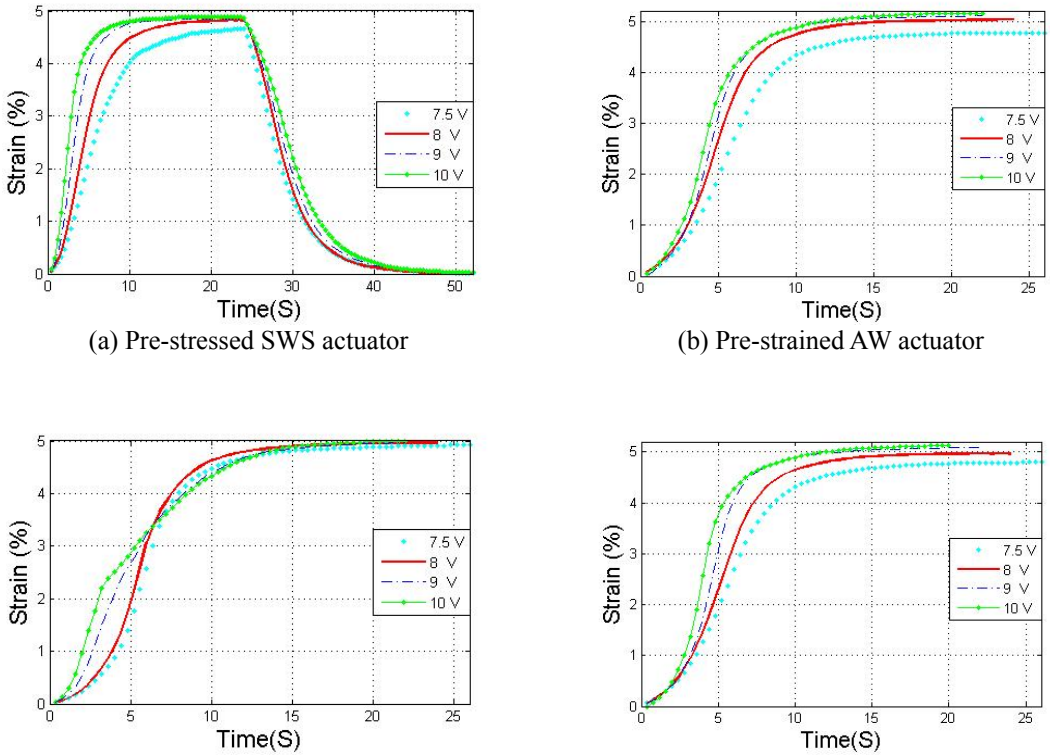

(a) Pre-stressed SWS actuator (b) Pre-strained AW actuator

(c) Pre-stressed AWS actuator (d) Pre-stressed AWSS actuator

Fig. 11 Responding speeds under different voltage

4.4 Resistance self-sensing control accuracy

A preview study (Lan and Fan 2010) showed that the inner stress determined the hysteresis gap between the heating and cooling loop of the S-R curve of the SMA wires. The minor loops and the major loops almost over lap when the gap is minimized, which makes the resistance feedback control model simple and accurate. Because the inner forces of the four actuators are not in the same magnitude, the S-R curve and the control response of every actuator are compared.

To achieve a wider recovered strain, sufficient stress was applied to the wires during driving. A polynomial model with one-to-one mapping might be sufficient to describe the path of the major loop of the S-R curve. To prove this solution, the MATLAB® "Polyfit" function was used to obtain the coefficients of the polynomials. Testing verified that seventh-order polynomials had sufficient accuracy. The approximate functions for the S-R curves are denoted as

$$R == a_1\varepsilon^7 + a_2\varepsilon^6 + a_3\varepsilon^5 + a_4\varepsilon^4 + a_5\varepsilon^3 + a_6\varepsilon^2 + a_7\varepsilon + a_8 \quad (1)$$

where R is the resistance of the SMA wires, ε is the displacement with respect to the original length of the austenitic SMA wire (strain), and a1-a7 refers to the coefficients of all orders. The

functions include the heating and the cooling paths of the SMA wires of all the actuators. The S-R curves of the two wires in the antagonistic actuators were symmetrical, which meant that one wire was enough. Fig. 12 gives the S-R curve and the modeling curves of the SMA wires in the different actuators. The corresponding modeling parameters are listed in Table 6.

As shown in Fig. 12, the modified heating and cooling paths were shifted by R = +0.05 and R = −0.05 and then plotted. According to the equation, once a target strain St has been targeted, the corresponding resistance RS will be compared with the self-sensed resistance to modify the output signal. Compared with the others, the S-R curves of the SWS and AWS actuators show wider gaps between the heating and the cooling paths, and this is caused by insufficient spring stiffness.

Multi-step response tests were carried out based on the function of seventh-order polynomials, Fig. 13 presents the measurement results for the LVDT, which shows the target signal and the control results, which were obtained using the resistance feedback PID control. The responses were tested after thirty cycles until the strain became more stable. The increment in each step was roughly 0.8% strain over 8 sec. The results showed that the resistance feedback model can achieve accurate responding in all four actuators. However, the SWS and AWS actuators showed comparatively worse accuracy, which was caused by insufficient inner stress.

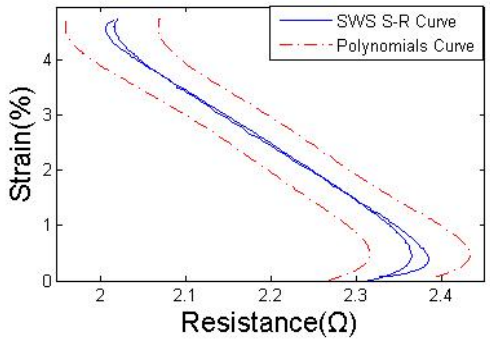

(a) Pre-stressed SWS actuator

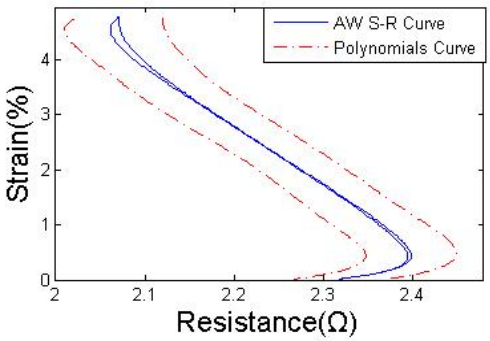

(b) Pre-strained AW actuator

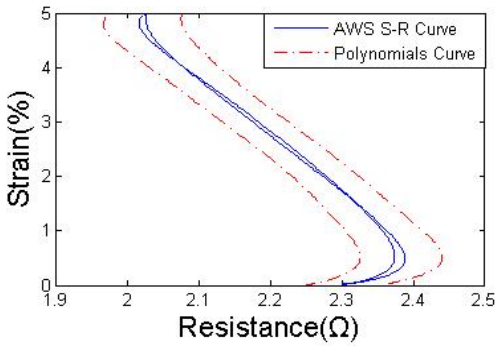

(c) Pre-stressed AWS actuator

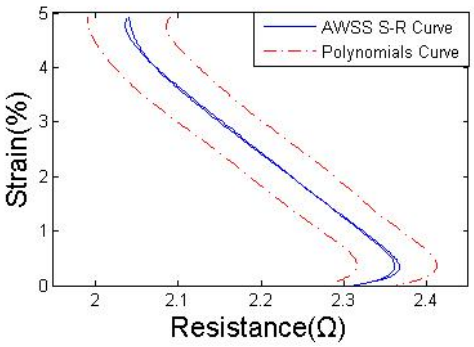

(d) Pre-stressed AWSS actuator

Fig. 12 The actual S-R curves and polynomials fitted curve

Table 6 Parameters for SMA S-R curve modeling

Path	a_1	a_2	a_3	a_4	a_5	a_6	a_7	a_8
SWS^h	0.0006	-0.0108	0.0807	-0.3153	0.6905	-0.8425	0.4305	2.3103
SWS^c	0.0004	-0.0067	0.0469	-0.1760	0.3842	-0.4994	0.2757	2.3129
AW^h	0.0004	-0.0071	0.0576	-0.2453	0.5847	-0.7744	0.4339	2.3667
AW^c	0.0009	-0.0160	0.1161	-0.4359	0.9066	-1.0350	0.5138	2.3592
AWS^h	0.0005	-0.0088	0.0671	-0.2655	0.5805	-0.6898	0.3227	2.3523
AWS^c	0.0003	-0.0052	0.0424	-0.1806	0.4264	-0.5491	0.2642	2.3643
$AWSS^h$	0.0009	-0.0182	0.1534	-0.6862	1.7413	-2.4924	1.7692	1.9396
$AWSS^c$	0.0001	-0.0031	0.0428	-0.2663	0.8670	-1.5115	1.2224	2.0576

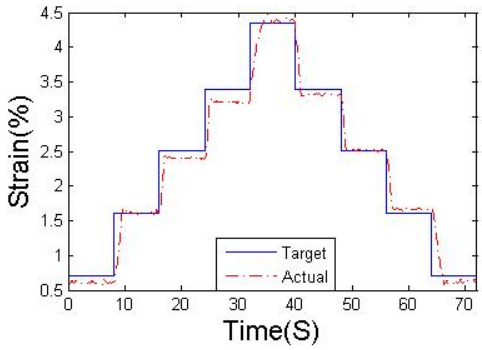

(a) Pre-stressed SWS actuator

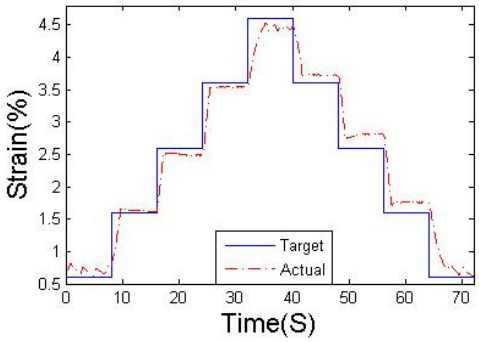

(b) Pre-strained AW actuator

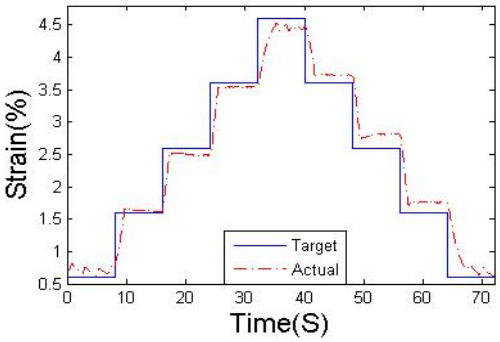

(c) Pre-stressed AWS actuator

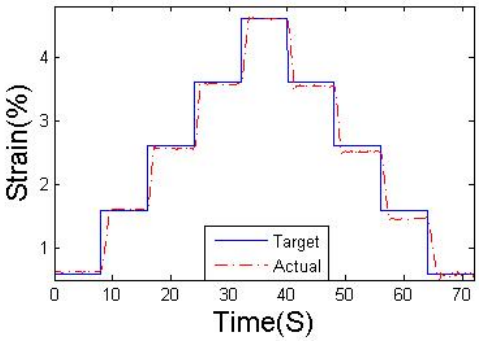

(d) Pre-stressed AWSS actuator

Fig. 13 The step-control results

Table 7 RMS errors of different actuators

RMSE	SWS	AW	AWS	AWSS
%	2.145	1.628	3.183	1.003

To study the difference between the target strain and the actual strain in all actuators, we used the root-mean-square error (RMSE) of the multi-step response to evaluate the accuracy of the models. The RMS tracking errors of the four actuators were 2.045%, 1.628%, 2.783%, and 1.003%, as shown in Table 7. Note that errors increase proportional to degradation.

4.5 Controllable maximum output (control accuracy under external interference)

To determine controllable maximum output, a few tests under external excitation were done during the step responding experiments, as shown in Fig. 14, which presents the measurements of the LVDT. Extra force was applied on the slider, from +10N to -10N, and the force direction are parallel to the linear bearing.

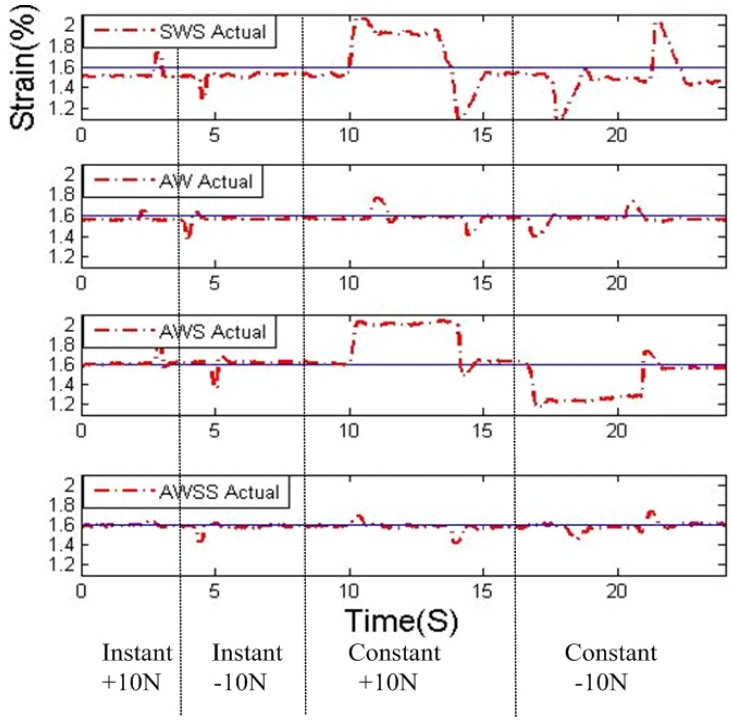

Fig. 14 Step-control results under interference of four actuators

The results show that with instantaneous disturbance under 10N, the slider of all actuators had 0.1%-0.2% strain wave, and over-shoot made an opposite wave of strain occur after the disturbance was removed. All interference was eliminated in 0.2 s with resistance feedback.

The condition was different under constant applied disturbance. In the AW and AWSS actuators, it was still possible to mitigate interference by resistance feedback control, but it needed more time, 0.8 s, to overcome the stronger applied force. In the SWS and AWS actuators, the low stiffness of the springs caused the unavailability of self-correction by resistance feedback. Although the wires still attempted to mitigate the disturbance, the extension of the springs cause terference was available for correction while the applied external force was pulling the wires, and it was unable to be rectified while the external force was pulling the springs. The disturbance could not be correct in both directions of the AWS actuator. A displacement of the slider of more than 0.4% cause it deviate from its target.

Note that the ability to resist interference depends on the diameter of the wire, which is limited by the materials stiffness. The diameter of the SMA wires should be chosen according to the force output requirement of the actuator. The control model did not show much change in diameter.

5. Conclusions

This paper studied the performance of four types of SMA actuators design, focusing on three antagonistic SMA actuators exhibiting two-way motion. The effect of pre-straining and spring stiffness was first investigated to obtain the maximum recovered strain. Actuation analysis was carried out first to determine the trend of these effects, which was then verified by the experiments. The initial parameters of the cyclic degradation analysis were chosen from the optimized condition of the recovered strain. The degradation of the AWS and AWSS actuators was shown to slow down after about 30 and 60 cycles of operation. The SWS and AW actuators showed significant degradation, which slow down after about 130 cycles. Different voltages were applied to the actuators to demonstrate the improvement in response speed of the antagonistic SMA-wires actuator. The results showed that the antagonistic SMA-wires actuator had faster response speed in two directions. In particular, the responding frequency of the AW and AWSS actuators increased to 0.13Hz with the voltage increased to 9V. A series of tests determined the control accuracy of the actuators by self-sensing feedback. Among all four actuators, the AW and AWSS actuators showed superior performance in precision with sufficient internal stress. To further demonstrate the performance of accurate control under interference, instant and constant disturbance were applied to the actuators. The AW and the AWSS actuators displayed high stability under external stress, whereas the SWS and the AWS actuators deviated from their targets under constant disturbance.

In summary, this paper applied the quantitative measure of the four actuators on five key properties, and the merits and deficiencies of each actuator are clarified. In the practical design of an actuator, the type of actuator should be chosen according to a suitable match between the performance and system requirements. Based on the results of the performance analysis, we expect that this study could provide an application basis for the design of SMA actuators.

Acknowledgments

This study was funded by the 863 National Key Foundation (2009AA045301) and National Natural Science Foundation of China (61175104).

References

Bundhoo, V., Haslam, E., Birch, B. and Park, E.J. (2008), *A shape memory alloy-based tendondriven actuation System for biomimetic artificial fingers*, Part I: Design and Evaluation, Cambridge University Press, Robotica.

Duerig, T.W., Melton, K.N., Stockel, D. and Wayman, C.M. (1990), *Engineering aspects of shape memory alloys*, UK: Butterworth-Heinemann.

Dynalloy, Inc. www.dynalloy.com/

Furuya, Y., Shimada, H., Matsumoto, M. and Honma, T. (1988), "Cyclic deformation and degradation in shape memory effect of Ti–Ni wire", *Jpn. Inst. Met*., **52**(2), 139-143.

Furuya, Y., Shimada, H., Matsumoto, M. and Honma, T. (1989), "Fatigue and degradation of shape memory effect in Ti–NiJ", *Proceedings of the MRS International Meeting on Advanced Materials*, Japan. 9.

Gall, K. and Maier, H.J. (2002), "Cyclic deformation mechanisms in precipitated NiTi shape memory alloys", *Acta Mater*., **50**(18), 4643-4657.

Hornbogen, E. (2004), "Thermo-mechanical fatigue of shape memory alloys", *J. Mater. Sci*., **39**, 385-399.

Kohl, M. (2004), *Shape Memory Microactuators*, Springer-Verlag, Berlin Heidelberg.

Kohl, M., Just, E., Pfleging, W. and Miyazaki, S. (2000), "SMA microgripper with integrated antagonism Sens", *Sensor. Actuat. A- Phys*., **83**, 208-213.

Kyung, J.H., Ko, B.G., Ha, Y.H. and Chung, G.J. (2008), "Design of a microgripper for micromanipulation of microcomponents using SMA wires and flexible hinges Sens", *Sensor. Actuat. A- Phys*., **141**(1), 144-150.

Lan, C.C. and Fan, C.H. (2010), "Investigation on pretensioned shape memory alloy actuators for force and displacement self-sensing", *Proceedings of the 2010 IEEE/RSJ International Conference on Intelligent Robots and Systems*, Taiwan.

Lan, C.C. and Fan, C.H. (2010), "An accurate self-sensing method for the control of shape memory alloy actuated flexures", *Sensor. Actuat. A- Phys*., **163**(1), 323-332.

Lan, C.C., Wang, J.H. and Fan, C.H. (2009), "Optimal design of rotary manipulators using shape memory alloy wire actuated flexures", *Sensor. Actuat. A- Phys*., **153**(2), 258-266.

Lan, C.C. and Yang, Y.N. (2009), "A computational design method for a shape memory alloy wire actuated compliant finger", *J. Mech. Design*, **131**(2), 021009.

Ma, N., Song, G. and Lee, H. (2004), "Position control of shape memory alloy actuators with internal electrical resistance feedback using neural networks", *Smart Mater. Struct*., **13**(4), 777-783.

Otsuka, K. and Wayman, C.M. (1998), *Shape Memory Materials*, Cambridge University Press, New York.

Romano, R. and Tannuri, EA. (2009), "Modeling, control and experimental validation of a novel actuator based on shape memory alloys", *Mechatronics*, **19**(7), 1169-1177.

Scherngell, H. and Kneissl, A.C. (1998), "Training and stability of the intrinsic two-way shape memory effect in Ni–Ti alloys", *Scripta Materialia*, **39**(2), 205-212.

Schiedeck, F. and Mojrzisch, S. (2011), "Design of a robust control strategy for the heating power of shape memory alloy actuators at full contraction based on electric resistance feedback", *Smart Mater. Struct*., **20**(4), 45002-45012 (11).

Sofla, A. Elzey, D. and Wadley, H. (2008), "Cyclic degradation of antagonistic shape memory actuated structures", *Smart Mater. Struct*., **17**(2), doi:10.1088/0964-1726/17/2/025014.

Song, G. (2007), "Design and control of a nitinol wire actuated rotary servo", *Smart Mater. Struct*., **16**(5), 1796-1801.

Sreekumar, M., Nagarajan, T. and Singaperumal, M. (2008), "Experimental investigations of the large deflection capabilities of a compliant parallel mechanism actuated by shape memory alloy wires", *Smart Mater. Struct*., **17**(6), 065025.

Teh, Y.H. and Featherstone, R. (2008), "An architecture for fast and accurate control of shape memory alloy actuators", *Int. J. Robot. Res*., **27**(5), 595-611.

Wang, T.M., Shi, Z.Y., Liu, D., Ma, C. and Zhang, Z.H. (2012), "An accurately controlled antagonistic

shape memory alloy actuator with self-sensing", *Sensors*, **12**(6), 7682-7700.
Wang, Z., Hang, G., Li, J., Wang, Y. and Xiao, K. (2008), "A micro-robot fish with embedded SMA wire actuated flexible biomimetic fin Sens", *Sensor. Actuat. A- Phys*., **144**, 354-360.

BS